metals

MDPI

Article

Study on Wear Resistance Evolution of Cold-Rolled Strip Flatness Meter Surface-Strengthened Layer

Shuai Zhang [1], Shuang Liao [1], Shan Li [1], Tongyuan Zhang [1], Huaxin Yu [1,2,*] and Hongmin Liu [1,2]

[1] National Engineering Research Centre for Equipment and Technology of Cold Rolling Strip, Yanshan University, Qinhuangdao 066004, China; m18633537842@163.com (S.Z.); 18281079605@163.com (S.L.); 15517975571@163.com (S.L.); 13180591081@163.com (T.Z.); liuhmin@ysu.edu.cn (H.L.)

[2] State Key Laboratory of Metastable Materials Science and Technology, Yanshan University, Qinhuangdao 066004, China

* Correspondence: yuhx@ysu.edu.cn; Tel.: +86-15033537589

Abstract: Seamless flatness rollers are the core equipment for cold-rolled strip flatness detection. The change in wear resistance of the roller surface-strengthened layer has important guiding significance for the prediction of the roller surface life. The experimental results of the five rounds of friction and wear testing show that the volume–wear rate of the original roller surface is only 1.85×10^{-6} mm^3 (N·M)$^{-1}$. After the first grinding, the wear resistance of the roller surface decreased and the wear rate was approximately 2.76×10^{-6} mm^3 (N·M)$^{-1}$. After the second grinding, the wear morphology, wear rate and wear resistance of the samples in each round showed little difference. The average wear rate in the last three rounds of the test is 3.56×10^{-6} mm^3 (N·M)$^{-1}$ and the wear resistance is significantly lower than that of the previous two rounds of the test. The calculation shows that the original surface wear resistance is 32.92% higher than that of the surface after the first grinding, and the average wear resistance of the surface after the first grinding is 22.59% higher than that of the surface after the second, third and fourth grinding. With long-term use and repeated grinding repair, the roller surface will show a trend of wear resistance decline. When the wear resistance decreases to a certain degree, it will reach a stage of stability. These phenomena provide regular and quantitative references for the study of the life prediction of flatness meter rollers.

Keywords: thin strip; flatness meter roller; strengthened layer thickness; wear resistance; volume wear rate

Citation: Zhang, S.; Liao, S.; Li, S.; Zhang, T.; Yu, H.; Liu, H. Study on Wear Resistance Evolution of Cold-Rolled Strip Flatness Meter Surface-Strengthened Layer. *Metals* **2023**, *13*, 914. https://doi.org/10.3390/met13050914

Academic Editor: Zbigniew Pater

Received: 4 April 2023
Revised: 28 April 2023
Accepted: 5 May 2023
Published: 8 May 2023

1. Introduction

The cold-rolled strip is one of the most important raw materials of industrial construction fields, which includes, but is not limited to, the usage of the integrated circuit of the bar, colour tube shield, battery plate, communication device, etc. [1]. With the rapid development of global aerospace, rail transit, communication information, and household appliances, the market has been raising the demand for all types of high-end cold-rolled thin strips [2–4]. The flatness of strip products intuitively refers to the warping degree of the strip and is the transverse uneven extension distribution of strip elongation. It is essentially the distribution of residual stress inside the strip and an important quality index of cold-rolled thin strip [5,6], which has a great impact on the yield of cold-rolled strip and the quality of subsequent deep-processing products. It is also an important technical index used to improve the added value of products and customer satisfaction. The flatness meter is the core equipment for flatness detection and closed-loop control [7,8]. After more than 30 years of research, Yanshan University has developed a seamless detection roller and built-in wireless flatness signal transmission processor [9,10], which constitutes the seamless flatness meter. The flatness meter has been successfully used in a series of industrial applications and achieved a good effect. A flatness meter can bring the gain of tens of millions of CNY annually. The seamless flatness meter is a whole-roller-type

equipment. The sensors are installed through holes 6 mm under the surface, and the surface is a complete cylinder [11]. This type of flatness meter does not affect the strip's surface quality and is easier to maintain than the segment-type, cylinder-sensor-type and insert-type flatness meters and is the future development trend of cold-rolling detection equipment [12].

The main point of user concern about the flatness meter is its direct economic benefits, followed by the service life and maintenance issues of the detecting part. The core detecting part of the flatness meter is the detection roller, which is the most valuable part of the equipment and the most difficult part to repair, so its service performance and service life should be focused on. The detection roller is installed before the strip coiler at the exit side of the cold-rolling mill, and the surrounding environment of the mill is complicated. There is a long-term pressure between the strip and the detection roller [13], and steel chips are generated and accumulate in the production process. The surface hardness and wear resistance are closely related to the life of the detection roller [14]. To ensure long-term stable online operation, the surface-strengthening method is adopted for the roller to obtain a higher hardness and good wear resistance to satisfy the requirements of the roller surface [15,16].

Friction and wear problems have always been the focus of surface science research [17–19]. Roller wear for steel rolling has always been a key problem in the metal-rolling process [20–22], and there have been many studies on work–roller wear. Li [23] changed the alloying element content of the work roller for cold rolling by adding 4% Cr and Ti elements. The wear and wear resistance of the work roller were experimentally studied. The test results showed that Ti changed the original friction form and improved the wear resistance of the original roller material by 175%. Anh Kiet Tieu et al. [24] studied the difference in wear resistance between the original surface of hot rolls in dry air and the surface oxide layer in wet air. The results showed that a high temperature makes the oxide skin peel off into the friction pair, resulting in great differences in the tribological characteristics of the two surfaces. Masayasu Ueno et al. [25] adopted the method of spark coating to improve the wear resistance of the roller surfaces and compared it with the conventional Cr plating coating. The results show that a hard layer with a Vickers hardness above Hv1500 can be formed when the TiC sintered electrode is used to discharge the 2% Cr steel, and it has better wear resistance than the conventional Cr-plating roller.

The seamless-detection roller is perforated 6 mm under the roller surface to install precision piezoelectric sensors, as shown in Figure 1a, which is the most significant difference from other rolling rollers [8–11]. To ensure that the surface of the detection roller does not crack when the sensors are installed, the depth of the strengthened layer of the roller is limited. Meanwhile, long-term use of the roller will cause surface wear, which decreases the surface finish, as shown in Figure 1b. The grinding roller is required to repair the roller surface. The grinding quantity is 0.2–0.3 mm in a single time, which further thins the strengthened layer and gradually changes the wear resistance. The surface repair is the most direct factor leading to the strengthened layer-thinning and the long-term friction with the strip may also affect the performance of the roller surface. In the process of grinding repair and long-term grinding with the strip, whether there is a qualitative or quantitative rule in the change of wear resistance of the roller surface is worth the attention of researchers and users. At present, there are many research results on the wear resistance of work rollers in the process of rolling production, but qualitative and quantitative analyses on the wear resistance of detection roller surfaces have not been studied. In this paper, the wear resistance values of the original surface of the detection roller and the restored surface of the grinding roller are experimentally compared, and the influence of the reduction of the strengthened layer-thickness on the wear resistance of the detection roller is analysed and calculated to provide a quantitative reference for the study of its life prediction.

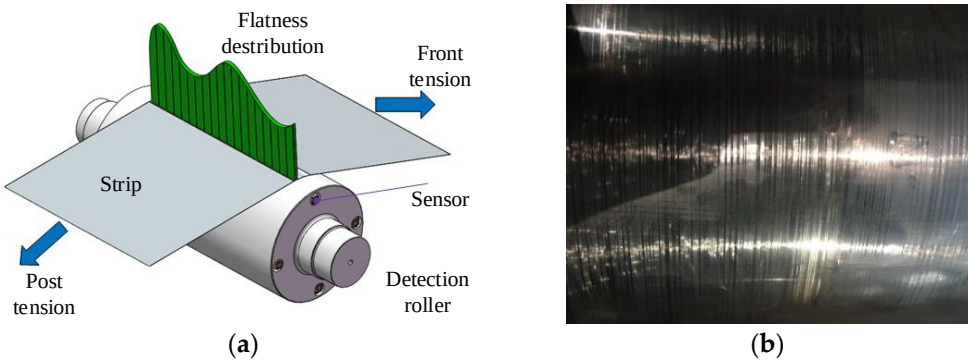

Figure 1. (**a**) Working principle and (**b**) surface wear of the detection roller.

2. Materials and Methods

2.1. Detection Roller Sample and Friction and Wear Testing Machine

When the detection roller is in normal operation, it basically runs online and does not leave the production line without problems. When the defects of the roller surface appear and are reflected on the strip surface, the mill needs to be stopped and the detection roller needs to be repaired by grinding. In order to simulate the actual working and repairing conditions of the roller and to obtain the evolution law of the wear resistance with the declining thickness of the hardened layer, the following experimental scheme is designed. Figure 2a shows the cut part of the Φ 300 mm detection roller, and the roller material is high carbon steel 9Cr_2MoV. The elements and content are shown in Table 1. In order to obtain the appropriate thickness and hardness of the strengthened layer, the heat treatment method of the roller surface is induction quenching at 9000 Hz of ultra-audio frequency and tempering at 195 °C for 30 h. The microhardness gradient on the surface of the detection roller is shown in Figure 2b. The surface thickness of the sample affected by the heat treatment is approximately 4 mm, within which the thickness of the part with a hardness of above 600 HV (55 HRB) is approximately 3.25 mm, and the maximum hardness is approximately 720 HV (61 HRB). The surface quenched layer is mainly martensite, and the matrix is pearlite. As shown in Figure 3, the MS-2A friction and wear testing machine can perform ring-block sliding friction experiments to record the load, friction torque, speed and friction coefficient in real time. The grinding ring material of the test is Cr_{12}MoV, which is installed on the outer port of the main shaft of the testing machine and synchronously rotates with the motor. The grinding sample of the experiment is the surface cut of the detection roller at the sample location, as shown in Figure 2a, which is placed in a special fixture. The sample is 30 mm long, 7 mm wide, and approximately 6 mm high.

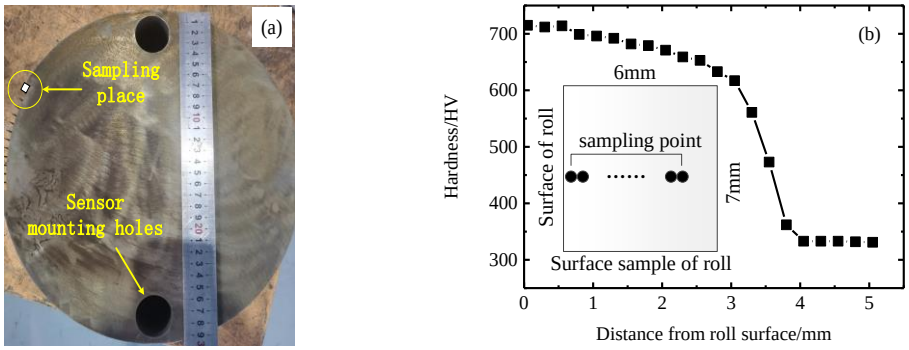

Figure 2. Samples and their hardness distribution: (**a**) Roller section and sampling location; (**b**) Hardness distribution along the radial direction of the roller.

Table 1. Element content of $9Cr_2MoV$(%).

Element	C	Si	Mn	P/S	Cr	Mo	V
Content	0.85~0.95	0.25~0.45	0.20~0.35	≤0.30	1.70~2.10	0.20~0.40	0.10~0.20

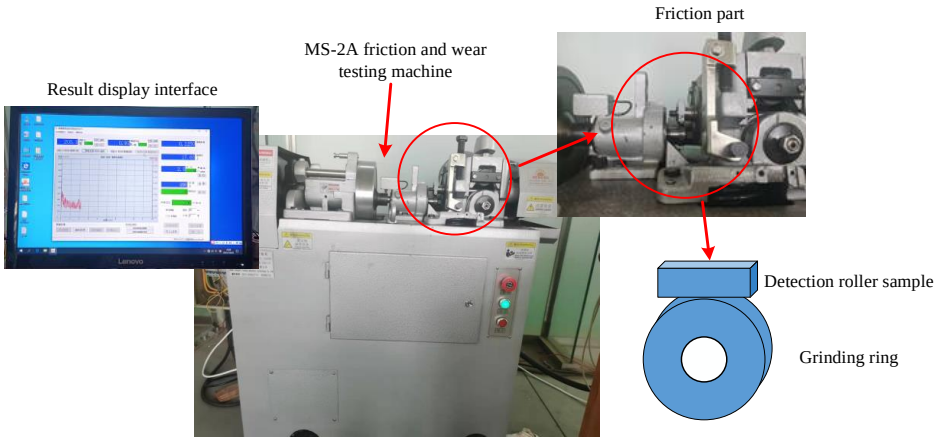

Figure 3. MS-2A friction and wear testing machine.

2.2. Test Scheme Design

In total, 13 detection roller surface samples are taken for 5 rounds of friction and wear tests and the diagram of the test process is shown in Figure 4. At the end of each round, one sample (No. 9–13) will be removed to measure the change in the strengthened layer hardness and excluded from the test process. The remaining samples were ground approximately 0.3 mm on the surface grinder before each round, and the next round of friction experiments was conducted. The last 8 samples (No. 1–8) will be used to statistically analyse the experimental results. The experimental parameters are unchanged for each round, as shown in Table 2.

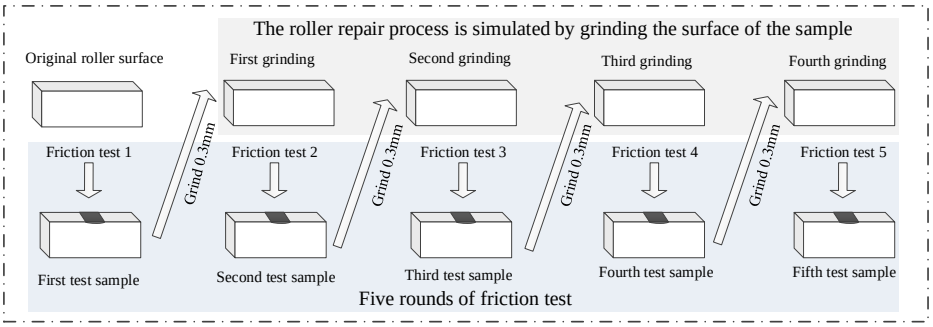

Figure 4. Diagram of five rounds of friction test.

Table 2. Friction and wear test parameters.

Load/N	Speed /r·min^{-1}	Time/min	Grinding Ring Material	Grinding Ring Hardness	Grinding Ring Diameter/mm	Temperature/°C	Lubrication
200	200	30	$Cr_{12}MoV$	55HRC	40	Room temperature	0.04 mL-Glycerin

2.3. Evaluation Methods for Wear Resistance

The friction coefficient is the ratio of the friction force between the sample and contact surface of the grinding part, to the positive pressure perpendicular to the sample surface, and can be directly obtained from the friction and wear experiment [26,27]. In the mutual friction process, the friction coefficient is a comprehensive characteristic of the friction pair,

which is affected by multiple factors, such as the rigidity, elastic geometric characteristics, sliding speed, humidity, temperature, and normal load of the friction pair [28,29]. Under identical experimental conditions, the friction coefficient is not related to the contact area but to the roughness of the contact surface. The wear morphology is an important basis to determine the wear mode. The wear morphology is magnified by scanning electron microscopy that can provide feedback on the wear condition and wear mode of the sample surface material and is one of the commonly used methods to characterize the wear resistance of the sample material [30–32]. Wear quantity, including volume wear quantity and mass wear quantity, is an important parameter to quantitatively characterize the wear resistance of specimens. Due to the small mass loss, it is difficult to accurately measure. In this paper, the volumetric wear rate is used to represent wear resistance. Formula (1) calculates the volumetric wear, and Formula (2) calculates the volumetric wear rate.

$$V = \left(\frac{1}{2} r^2 \arccos \frac{2r^2 - w^2}{2r^2} - \frac{1}{2} w \sqrt{r^2 - \frac{w^2}{4}} \right) b \tag{1}$$

where V is the wear volume; w is the width of the sample wear mark; r is the radius of the grinding ring, and r = 20 mm; b is the length of the sample, and b = 7 mm. The volume wear rate K is:

$$K = \frac{V}{FT} \tag{2}$$

where F is the pressure load (N), and T is the sliding stroke (m).

3. Results

3.1. Friction Coefficient Result

Figures 5–9 show the friction coefficients of samples No. 1–8 after five rounds of friction and wear experiments. The friction coefficients are basically stable at 0.2, and the wear patterns are basically identical. However, the friction coefficients sometimes dramatically change because the surface materials fall off, and the abrasive particles remain in the friction system during the friction process, which makes the experimental curves of some samples fluctuate. Figure 5 shows the friction and wear curves of the original surface layer of the eight samples in the first round of the test. The initial running-in stage takes approximately 2.5 min. The friction coefficients of samples No. 1, No. 2, No. 4, No. 5, and No. 7 have abrupt changes, and samples No. 2, No. 4, and No. 5 briefly return to a stable wear state. The friction coefficients of samples No. 3, No. 6, and No. 8 are very stable during the entire process. Figure 6 shows the curves of the second round of experiments after the samples are ground approximately 0.3 mm on the surface grinder. The friction coefficient curve basically follows the same pattern. Most of the samples have several abrupt changes in the friction coefficient during the experiment, and the curve finally returns to a stable state. As shown in Figure 7, except for sample No. 1, the friction coefficients of the other samples are basically identical, and there are several small mutations in the friction coefficients during the friction process. Figure 8 shows the fourth test curve of the samples after grinding with a surface grinder for a thickness of approximately 0.9 mm. The friction coefficient of samples No. 4, No. 5, and No. 7 decreased approximately 25 min later, which indicates that the friction torque changes after this time and the roughness of the contact surface begins to decline. The friction coefficient stabilizes at 0.2 at the beginning and drops below 0.2 later. Figure 9 shows the fifth test curve of the samples after grinding with a surface grinder to a thickness of 1.2 mm. The friction coefficients of samples No. 1, No. 2, No. 3, No. 4, and No. 5 slightly decrease in the later stage.

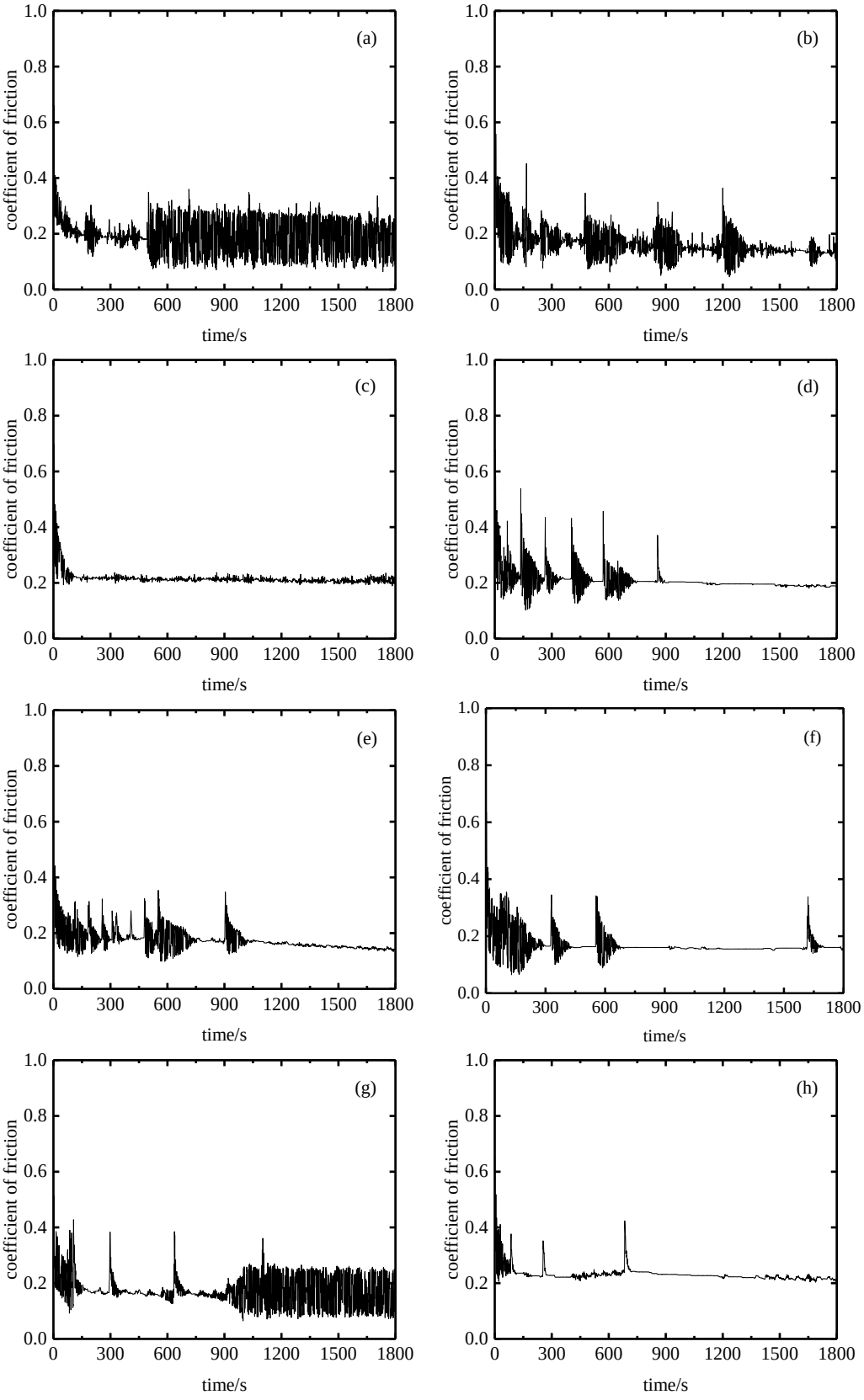

Figure 5. Friction coefficient curve of the first round of the friction test: (**a**) Sample No. 1; (**b**) Sample No. 2; (**c**) Sample No. 3; (**d**) Sample No. 4; (**e**) Sample No. 5; (**f**) Sample No. 6; (**g**) Sample No. 7; (**h**) Sample No. 8.

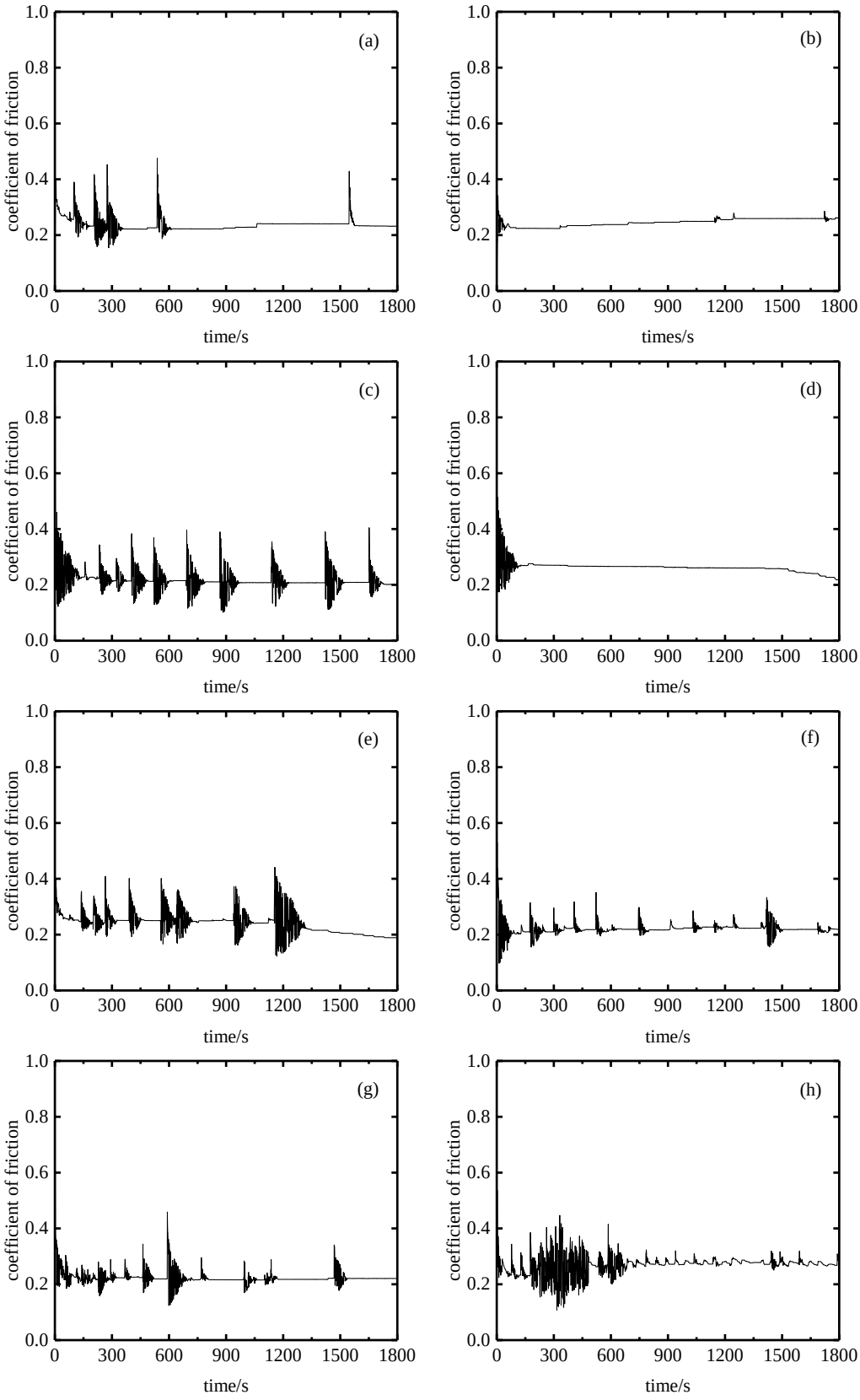

Figure 6. Friction coefficient curve of the second round of the friction test: (**a**) Sample No. 1; (**b**) Sample No. 2; (**c**) Sample No. 3; (**d**) Sample No. 4; (**e**) Sample No. 5; (**f**) Sample No. 6; (**g**) Sample No. 7; (**h**) Sample No. 8.

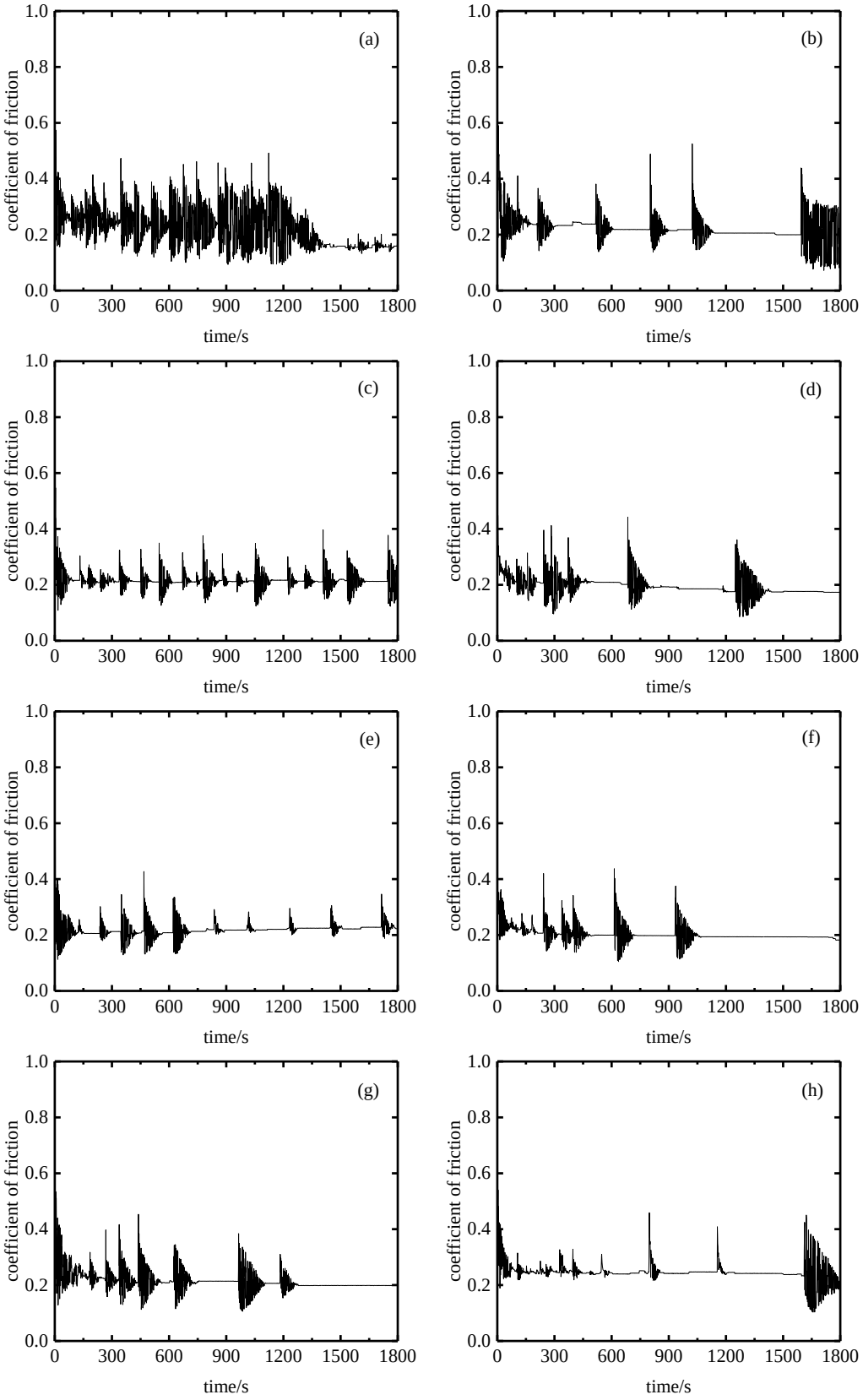

Figure 7. Friction coefficient curve of the third round of the friction test: (**a**) Sample No. 1; (**b**) Sample No. 2; (**c**) Sample No. 3; (**d**) Sample No. 4; (**e**) Sample No. 5; (**f**) Sample No. 6; (**g**) Sample No. 7; (**h**) Sample No. 8.

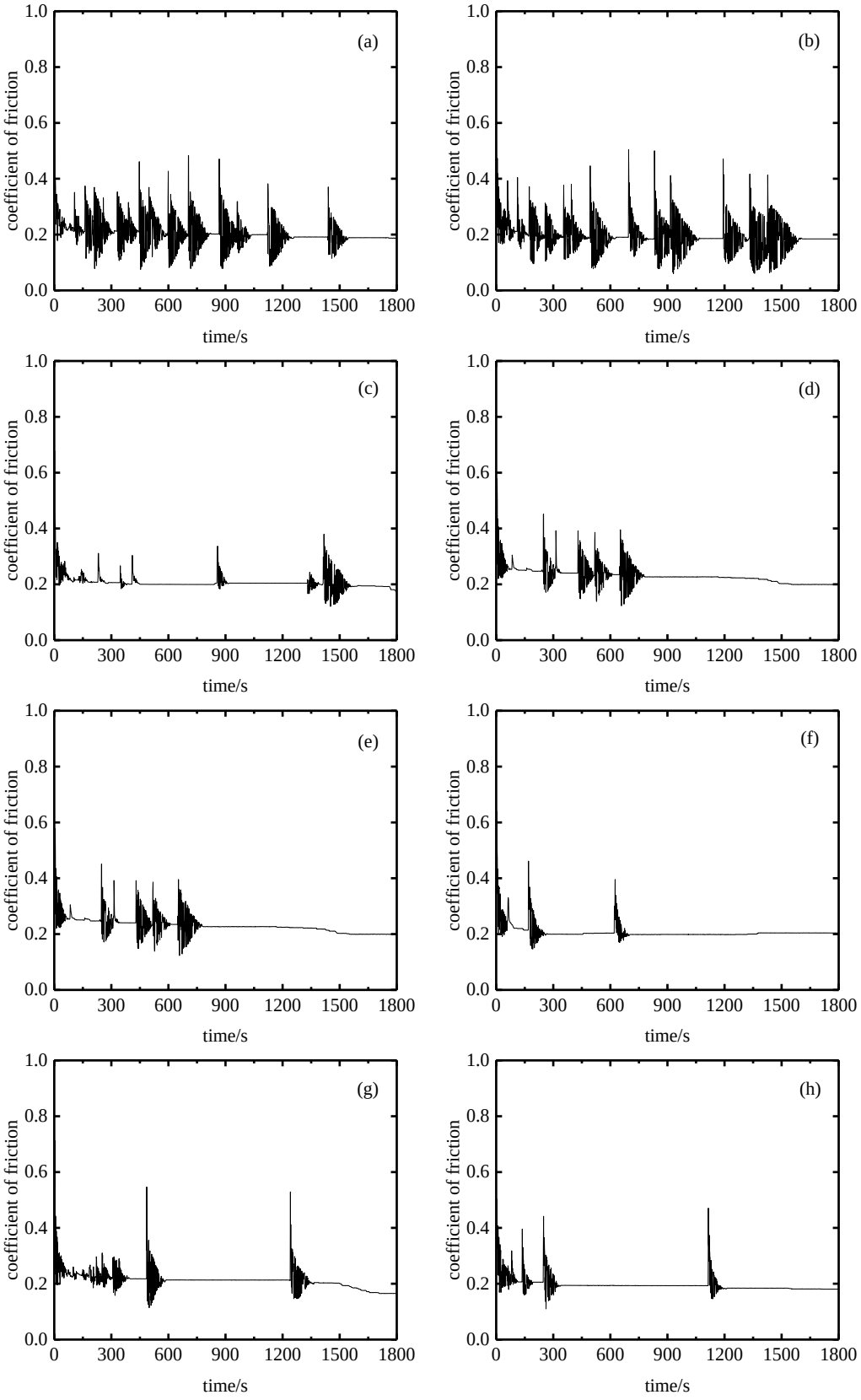

Figure 8. Friction coefficient curve of the fourth round of the friction test: (**a**) Sample No. 1; (**b**) Sample No. 2; (**c**) Sample No. 3; (**d**) Sample No. 4; (**e**) Sample No. 5; (**f**) Sample No. 6; (**g**) Sample No. 7; (**h**) Sample No. 8.

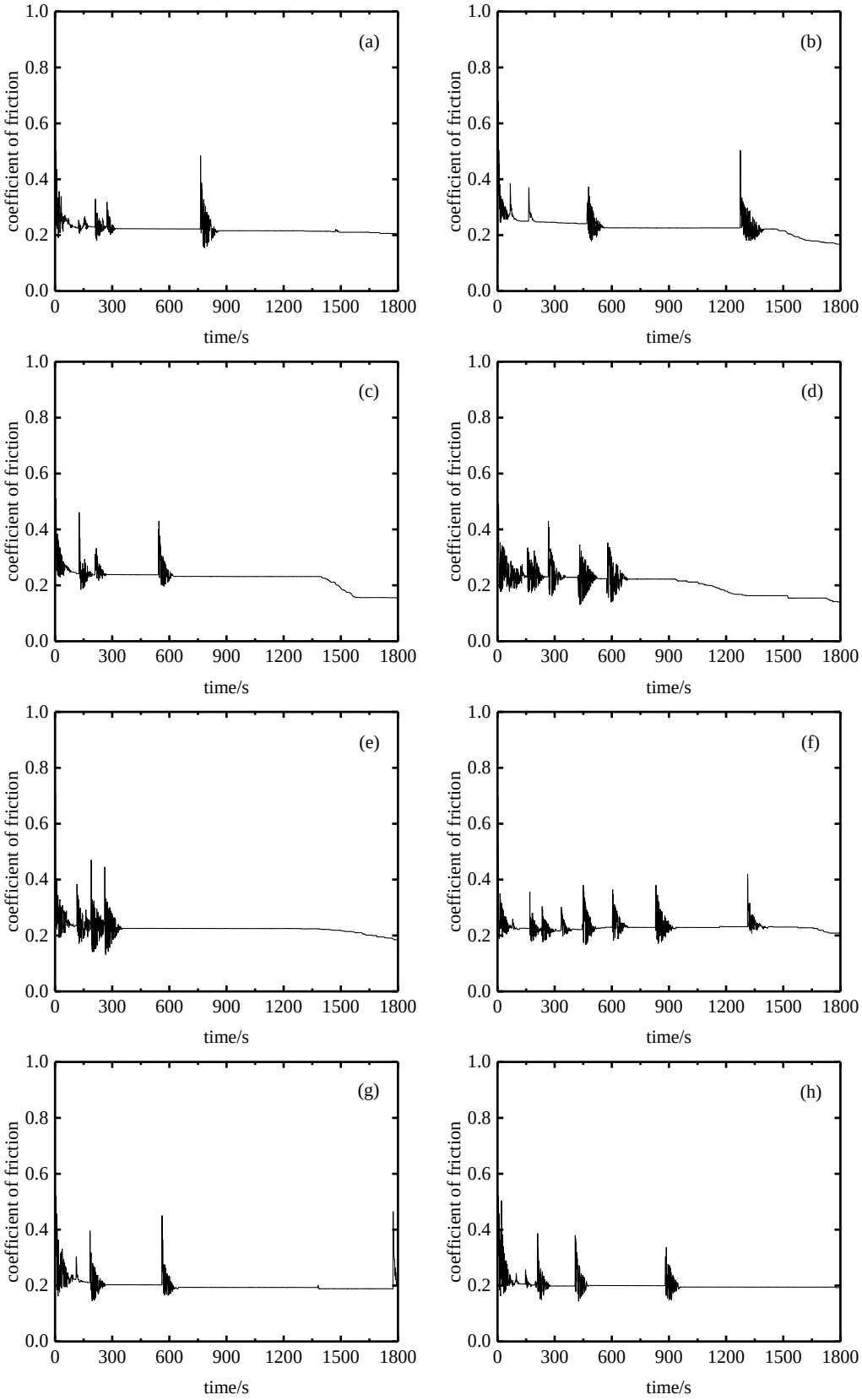

Figure 9. Friction coefficient curve of the fifth round of the friction test: (**a**) Sample No. 1; (**b**) Sample No. 2; (**c**) Sample No. 3; (**d**) Sample No. 4; (**e**) Sample No. 5; (**f**) Sample No. 6; (**g**) Sample No. 7; (**h**) Sample No. 8.

3.2. Comparison of Wear Morphology

Figure 10 shows the wear morphology of the original surface layer of the eight samples after the first round of the experiment. There is a deep furrow in image No. 5, while the wear degree of other images is low, basically abrasive wear, and the furrow is uniform. Figure 11 shows the wear morphology after the second round of tests. Compared with the results of the first round, the wear degree of the samples is intensified, and the furrows on each sample are deepened, but sample No. 4 retains a certain degree of adhesive wear. Figure 12 shows the wear morphology after the third round of tests. Compared with the second round, the wear of the image is significantly aggravated, the furrows are deeper, and the adhesion wear of No. 4 is more severe. Cracks appeared on the surface of samples No. 6 and No. 7, and the surface cracks disappeared after being ground by a grinder for 0.3 mm, which indicates that the cracks were only on the surface of the sample. As shown in Figures 13 and 14, the wear morphology of the fourth and fifth rounds is similar to that of the third round, with deep furrows and surface cracks.

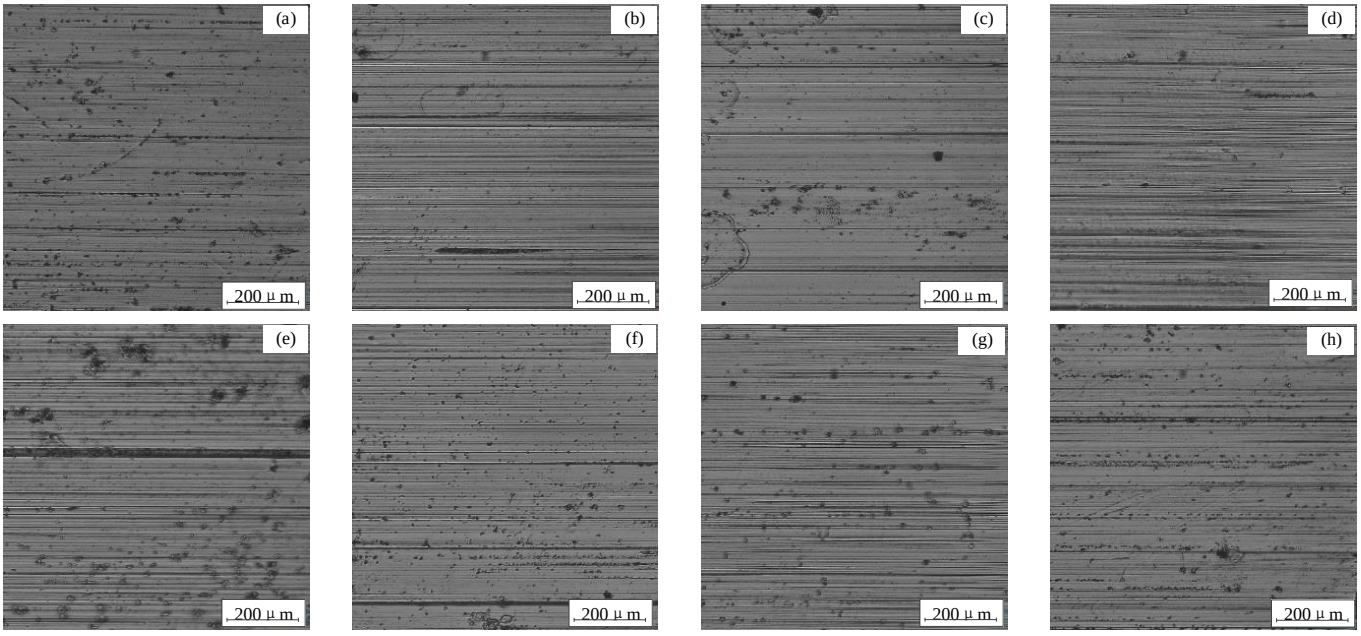

Figure 10. Wear morphology of the first round of the friction test: (**a**) Sample No. 1; (**b**) Sample No. 2; (**c**) Sample No. 3; (**d**) Sample No. 4; (**e**) Sample No. 5; (**f**) Sample No. 6; (**g**) Sample No. 7; (**h**) Sample No. 8.

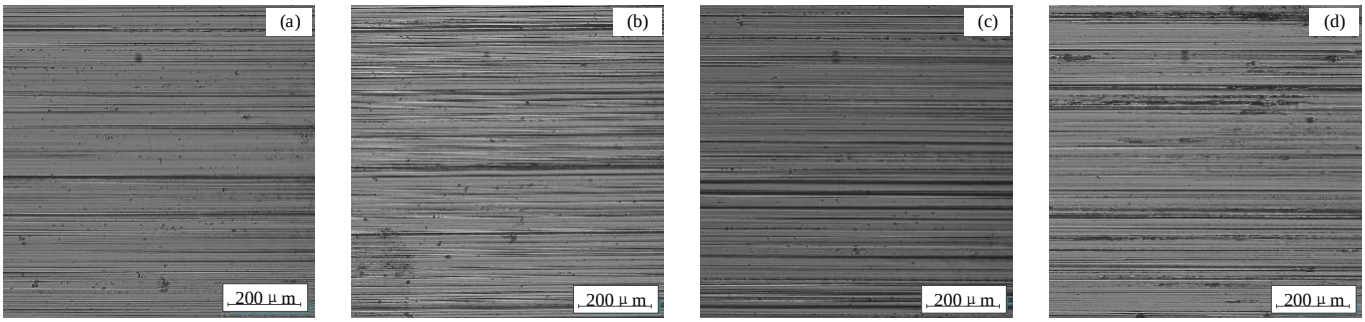

Figure 11. *Cont.*

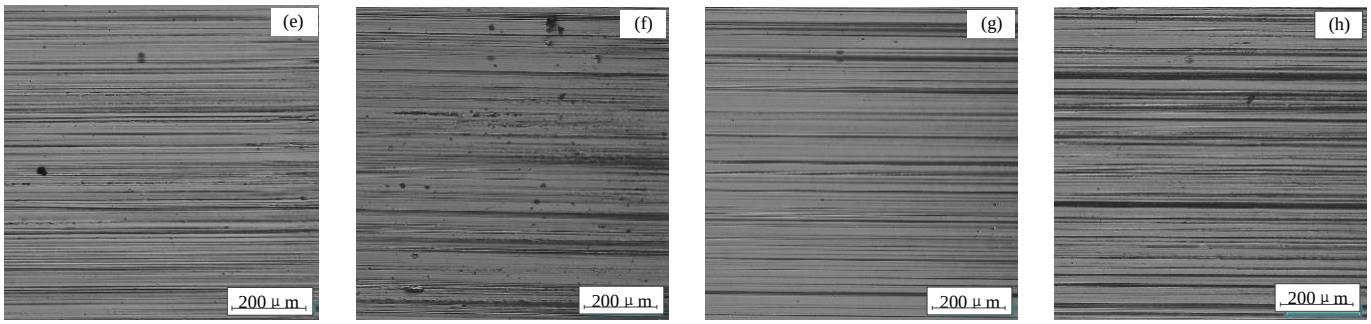

Figure 11. Wear morphology of the second round of the friction test: (**a**) Sample No. 1; (**b**) Sample No. 2; (**c**) Sample No. 3; (**d**) Sample No. 4; (**e**) Sample No. 5; (**f**) Sample No. 6; (**g**) Sample No. 7; (**h**) Sample No. 8.

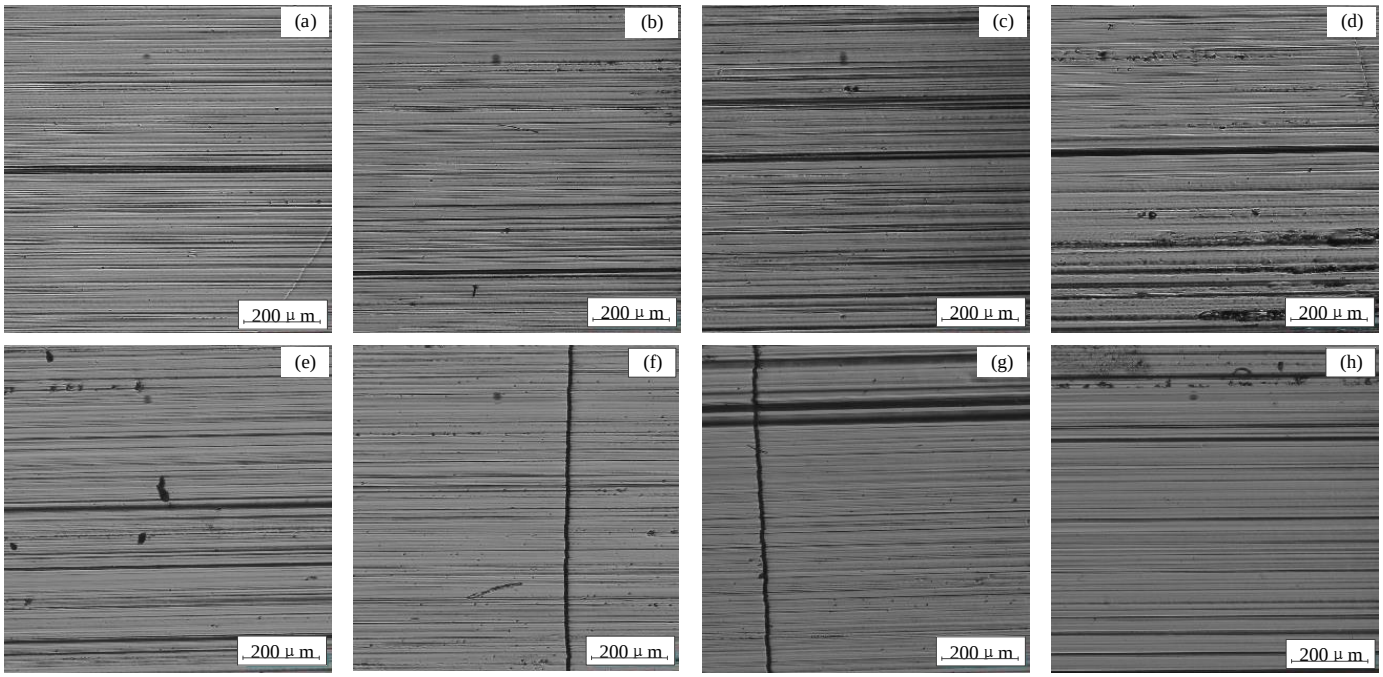

Figure 12. Wear morphology of the third round of the friction test: (**a**) Sample No. 1; (**b**) Sample No. 2; (**c**) Sample No. 3; (**d**) Sample No. 4; (**e**) Sample No. 5; (**f**) Sample No. 6; (**g**) Sample No. 7; (**h**) Sample No. 8.

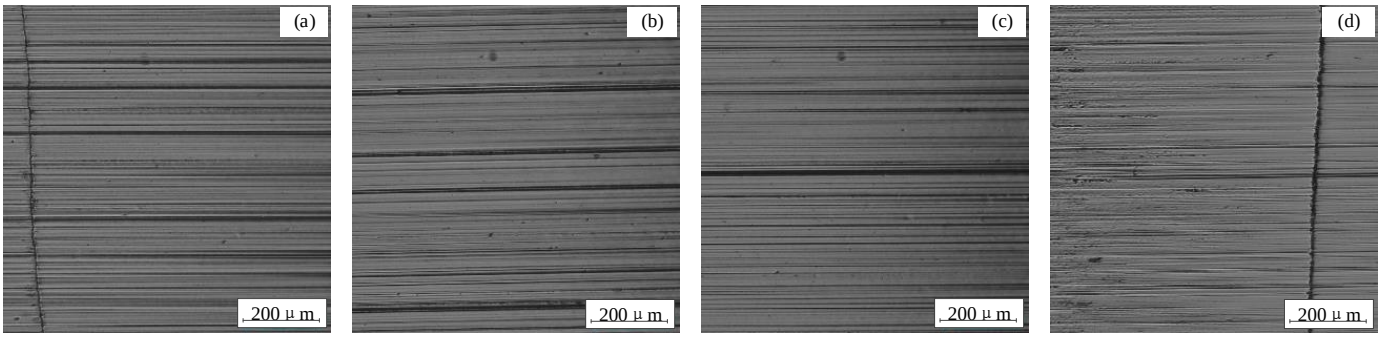

Figure 13. *Cont*.

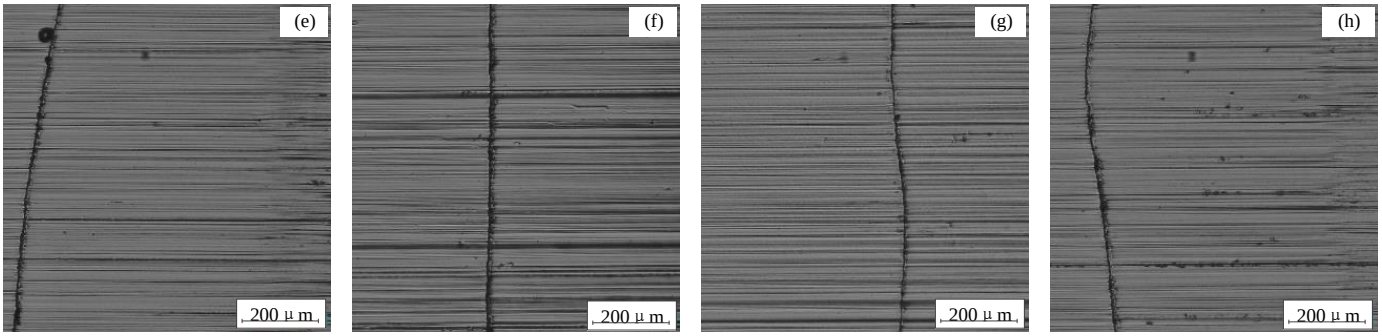

Figure 13. Wear morphology of the fourth round of the friction test: (**a**) Sample No. 1; (**b**) Sample No. 2; (**c**) Sample No. 3; (**d**) Sample No. 4; (**e**) Sample No. 5; (**f**) Sample No. 6; (**g**) Sample No. 7; (**h**) Sample No. 8.

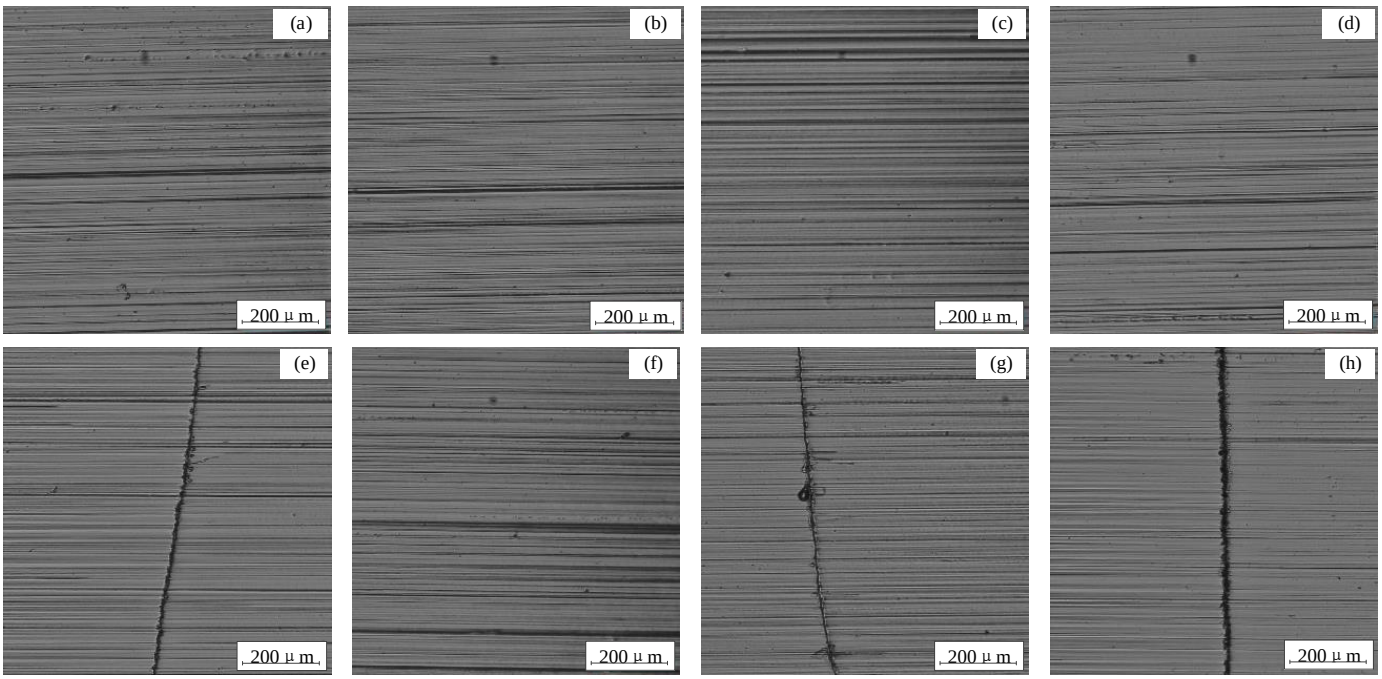

Figure 14. Wear morphology of the fifth round of the friction test: (**a**) Sample No. 1; (**b**) Sample No. 2; (**c**) Sample No. 3; (**d**) Sample No. 4; (**e**) Sample No. 5; (**f**) Sample No. 6; (**g**) Sample No. 7; (**h**) Sample No. 8.

3.3. Wear Result

The comparison of the wear mark width and the wear rate in five rounds of tests is shown in Figure 15. The wear mark width is compared in Figure 15a. In the first round of the test, the original surface has the smallest wear mark width, and the second round has an increased wear mark width. The wear mark width of the last three rounds is almost identical, which is wider than that of the first two tests and consistent with the observed wear morphology result. According to the calculation results of the wear rate in Figure 15b, the original surface has the best wear resistance, followed by the second round, and subsequent rounds have basically identical wear resistance. The wear resistance of the original surface layer is 32.92% better than that of the surface layer after one round of testing. The wear resistance of the surface layer after one round of testing was 22.59% better than that of the surface layer after two rounds of testing. The wear resistance of the surface layer after two rounds of testing is not dissimilar from that of the third and fourth rounds.

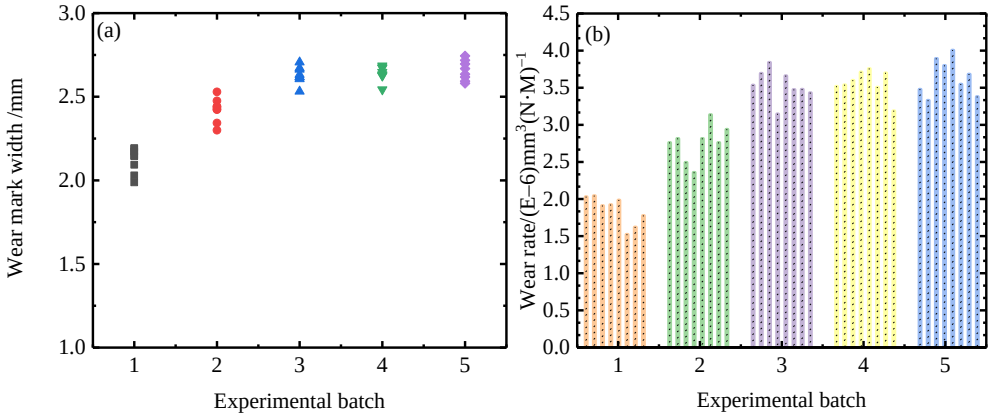

Figure 15. Comparison of the wear mark width and wear rate of the samples after each round of friction test: (**a**) wear mark width; (**b**) wear rate.

4. Discussion

A schematic diagram of wear theory is shown in Figure 16. When two contact surfaces wear out in the friction process, dislocation will occur on the surface of the material, which is called the plastic deformation zone. Due to the emergence of plastic deformation, the internal dislocation density gradually increases, or even exceeds the surface dislocation density, and dislocation plugs occur at a certain depth in the subsurface layer, which results in vacancy or crack formation [33,34]. The figure shows the curve of the plastic deformation degree according to the surface depth. The friction and wear process reduces the plasticity and toughness of the material and increases the residual stress, which is the main reason for the crack. According to the stress field analysis, the normal stress on the surface prevents the crack from spreading to the depth direction [35,36], so the crack is generally developed on the surface. After testing, the cracks disappear after a small amount of grinding machine processing, which implies that all cracks are on the surface.

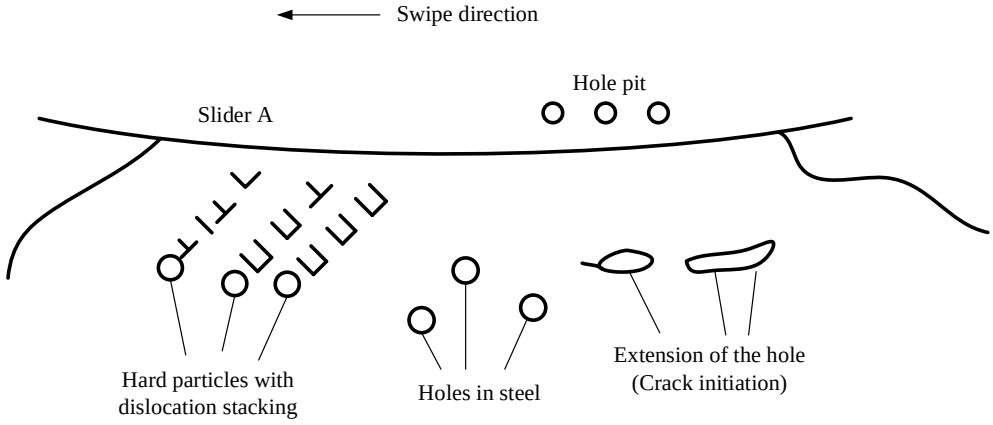

Figure 16. Schematic diagram of wear theory.

After the first round of testing, there is no plastic deformation on the surface of the sample. The material can absorb more energy than the subsequent tests, and it is difficult to form cracks and fatigue shedding, so it has better wear resistance than the subsequent rounds of testing. The experimental conditions of the last four wheels were almost identical. The plastic deformation area was still not completely worn off after the surface layer was ground off approximately 0.3 mm each time, and part of the deformation area in the plastic extension direction was retained. Therefore, the latter four rounds have lower wear resistance than the first round, but there is little difference between them.

As shown in Figure 17, after each round of tests, the hardness of the surface layer decreased due to severe wear, while the hardness of the subsurface layer increased due to

plastic deformation. There is little difference in the surface hardness of the samples after each grinding of 0.3 mm. After the last three rounds of grinding, the samples have a slightly higher surface hardness than the original surface. Through the wear theory analysis, it is not difficult to see that the plastic deformation zone affected by friction will remain at a certain thickness after grinding, which mainly affects the wear resistance of the surface of the detection roller.

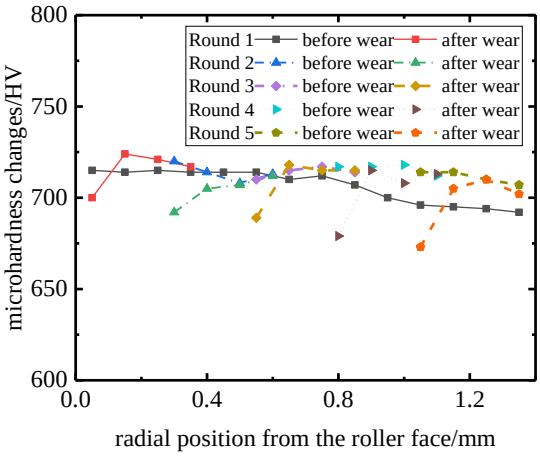

Figure 17. Changes in the microhardness of the samples after each round of the friction test.

5. Conclusions

The roller material in the test is $9Cr_2MoV$. After surface quenching, the hardness of the strengthened layer reaches 61 HRC, and the effective strengthened layer thickness is 3.25 mm. Its wear resistance is good. After the first round of 30 min of intense friction, the volume wear rate of the sample is only 1.85×10^{-6} mm^3 (N·M)$^{-1}$. The original surface condition of the roller that has not been used or worn on the line has a good working performance.

All friction coefficients of the five rounds of friction and wear tests are stable at approximately 0.2 with little variation. The wear morphology of the first and second tests is abrasive wear. The furrow depth is shallow, and no cracks occur in the samples. After the last three rounds of tests, obvious furrows and surface cracks appear in some samples.

The wear resistance of the original surface layer is 32.92% better than that of the surface layer after the first round of testing. The wear resistance of the surface after the first round of testing is 22.59% better than that after the second round of testing. The surface layer after the second round of testing has a similar wear resistance to that after the third and fourth rounds of tests.

The original surface wear resistance of the flatness meter roller is the highest. After long-term use and grinding repair, the surface wear resistance of the roller will be reduced. With the repeated use and repair of the roller, the wear resistance will gradually decline and will not change for a long period after declining to a certain extent and reach a steady state. The above phenomena have a guiding significance in the life prediction of the cold-rolled strip flatness meter roller.

Author Contributions: Conceptualization, S.Z. and H.Y.; methodology, H.Y.; validation, S.Z., S.L. (Shuang Liao) and S.L. (Shan Li); formal analysis, S.L. (Shuang Liao); writing—original draft preparation, S.Z.; writing—review and editing, S.L. (Shan Li).; visualization, T.Z.; project administration, H.L.; funding acquisition, H.L. All authors have read and agreed to the published version of the manuscript.

Funding: This research was funded by the National Natural Science Foundation of China, grant number U21A20118 and National Key R&D Program of China, grant number 2021YFB3401004 and "Giant Plan" innovation team and Leading Talents Fund of Hebei Province of China, grant number 4570019.

Data Availability Statement: Not applicable.

Acknowledgments: The studies were carried out on the equipment of the National Engineering Research Center for Equipment and Technology of Cold Rolling Strip and State Key Laboratory of Metastable Materials Science and Technology of Yanshan University.

Conflicts of Interest: The authors declare no conflict of interest.

References

1. Hao, L.; Ji, X.; Zhang, G.; Zhao, W.; Sun, M.; Peng, Y. Carbide precipitation behavior and mechanical properties of micro-alloyed medium Mn steel. *J. Mater. Sci. Technol.* **2020**, *47*, 122–130. [CrossRef]
2. Klinkenberg, C.; Kintscher, B.; Hoen, K.; Reifferscheid, M. More than 25 Years of Experience in Thin Slab Casting and Rolling Current State of the Art and Future Developments. *Steel Res. Int.* **2017**, *88*, 1700272. [CrossRef]
3. Qin, F.; Li, Y.; Qi, H.; Ju, L. Advances in Compact Manufacturing for Shape and Performance Controllability of Large-scale Components—A Review. *Chin. J. Mech. Eng.* **2017**, *30*, 7–21. [CrossRef]
4. You, X.; Wang, C.; Huang, J.; Gao, X.; Zhang, Z.; Wang, M.; Huang, Y.; Zhang, C.; Jiang, Y.; Wang, J.; et al. Towards 6G wireless communication networks: Vision, enabling technologies, and new paradigm shifts. *China Inf. Sci.* **2021**, *64*, 110301. [CrossRef]
5. Lian, J.; Liu, H. *Shape and Thickness Control*, 1st ed.; Weapon Industry Press: Beijing, China, 1995.
6. Wang, G. *Flatness Control and Flatness Theory*, 1st ed.; Metallurgical Industry Press: Beijing, China, 1986.
7. Qu, H.; Gu, T.; Fang, B. Research on development of surface-roughness variation and control technology of the automotive plates and rolls. *Baosteel Tech. Res.* **2019**, *13*, 8–19.
8. Wang, D.; Liu, H.; Liu, J. Research and Development Trend of Shape Control for Cold Rolling Strip. *Chin. J. Mech. Eng.* **2017**, *30*, 1248–1261. [CrossRef]
9. Yu, B.; Yang, L.; Liu, H.; Peng, Y.; You, L. Development and industrial application of cold-rolled strip steel contact shape meter. *Chin. J. Sci. Instrum.* **2010**, *31*, 904–911. [CrossRef]
10. Liu, H.; Liu, J.; Yu, B.; Yang, L.; Zhang, Y. Whole roll wireless shape meter and intelligent shape control system for strip cold rolling mill. *Chin. J. Mech. Eng.* **2017**, *53*, 87–93. [CrossRef]
11. Yu, H.; Liu, H.; Xu, Y.; Wang, D. Interpretation of the Chinese standard of cold-rolled strip flatness measurement and control system. *J. Iron Steel Res. Int.* **2019**, *54*, 52–57. [CrossRef]
12. Yu, B.; Yang, L.; Sun, J. Research status of cold-rolled strip flatness detection roller. *J. Iron Steel Res. Int.* **2011**, *28*, 44–46. [CrossRef]
13. Wang, P.; Zhang, D.; Liu, J.; Wang, J.; Yu, X. Research and Application of Calculation Model of Cold-rolled Plate Shape Measurement. *Chin. J. Mech. Eng.* **2011**, *47*, 58–65. [CrossRef]
14. Yu, H.; Zhang, T.; Zhang, S.; Wang, D.; Liu, H. Quick Recognition and Elimination of an Additional Signal Caused by Deflection of an Integral Roller Flatness Meter: Instrumentation, Control and System Engineering. *ISIJ Int.* **2021**, *61*, 2571–2579. [CrossRef]
15. Mevec, D.G.; Raninger, P.; Prevedel, P.; Jászfi, V. A Posteriori Reconstruction of the Temperature Distribution in Surface Hardened Tempering Steel. *Sci. Rep.* **2020**, *10*, 7481. [CrossRef] [PubMed]
16. Sun, S.; Liu, W.; Zhang, X.; Wan, M. Crankshaft HCF Research Based on the Simulation of Electromagnetic Induction Quenching Approach and a New Fatigue Damage Model. *Metals* **2022**, *12*, 1296. [CrossRef]
17. Ebrahimi, M.; Wang, Q. Accumulative roll-bonding of aluminum alloys and composites: An overview of properties and performance. *J. Mater. Res. Technol.* **2022**, *19*, 4381–4403. [CrossRef]
18. Wu, J.; Djavanroodi, F.; Gode, C.; Ebrahimi, M.; Attarilar, S. Microstructure evolution, texture development, and mechanical properties of hot-rolled 5052 aluminum alloy followed by annealing. *Mater. Res. Express* **2022**, *9*, 056516. [CrossRef]
19. Xu, H.; He, T.; Zhong, N.; Zhao, B.; Liu, Z. Transient thermomechanical analysis of micro cylindrical asperity sliding contact of SnSbCu alloy. *Tribol. Int.* **2022**, *167*, 107362. [CrossRef]
20. Servin-Casta, E.R.; Garcia-Lara, A.M.; Mercado-Solís, R.D.; Vega-Lebrun, C.A. Development of Mathematical Model for Control Wear in Backup Roll for Hot Strip Mill. *J. Iron Steel Res. Int.* **2014**, *21*, 46–51. [CrossRef]
21. Li, W. Simulation-based multi-objective optimization for roll shifting strategy in hot strip mill. *J. Cent. South Univ.* **2013**, *20*, 1226–1234. [CrossRef]
22. Jia, S.; Li, W.; Liu, X.; Du, B. Multi-Objective Load Distribution Optimization for Hot Strip Mills. *J. Iron Steel Res. Int.* **2013**, *20*, 27–32. [CrossRef]
23. Li, H.; Jiang, Z.; Tieu, A.K.; Wei, D. Experimental study on wear and friction of work roll material with 4% Cr and added Ti in cold rolling. *Wear* **2011**, *271*, 2500–2511. [CrossRef]
24. Tieu, A.K.; Zhu, Q.; Zhu, H.; Lu, C. An investigation into the tribological behaviour of a work roll material at high temperature. *Wear* **2011**, *273*, 43–48. [CrossRef]
25. Ueno, M.; Fujita, N.; Kimura, Y.; Nakata, N. Evaluation of coating and wear characteristics of roll surface coated with TiC by electrical discharge coating. *J. Mater. Process Technol.* **2016**, *236*, 9–15. [CrossRef]
26. Xu, B.; Zhu, S. *The Theory and Technology of Surface Engineering*, 2nd ed.; Beijing National Defense Industry Press: Beijing, China, 2010.
27. Azushima, A.; Yoneyama, S.; Utsunomiya, H. Coefficient of friction at interface of lubricated upsetting process. *Wear* **2012**, *286*, 3–7. [CrossRef]
28. Meng, Y.; Xu, J.; Jin, Z.; Prakash, B.; Hu, Y. A review of recent advances in tribology. *Friction* **2020**, *8*, 221–300. [CrossRef]

29. Liu, Z. *Principles of Tribology*, 1st ed.; Higher Education Press: Beijing, China, 2009.
30. Graves, A.; Norgren, S.; Wan, W.; Singh, S.; Kritikos, M.; Xiao, C.; Crawforth, P.; Jackson, M. On the mechanism of crater wear in a high strength metastable β titanium alloy. *Wear* **2021**, *484*, 203998. [CrossRef]
31. Goel, N.; Fong, T.M.; Shingledecker, J.P.; Russell, A.; Keller, M.W.; Shirazi, S.A.; Otanicar, T. Effect of temperature on abrasion erosion in particle based concentrating solar powerplants. *Sol. Energy* **2021**, *224*, 1127–1135. [CrossRef]
32. Xi, L.; Guo, S.; Ding, K.; Prashanth, K.G.; Sarac, B.; Eckert, J. Effect of nanoparticles on morphology and size of primary silicon and property of selective laser melted Al-high Si content alloys. *Vacuum* **2021**, *191*, 110405. [CrossRef]
33. Xu, C.; Li, P. Stress-free manufacturing technology. *Chin. J. Mech. Eng.* **2020**, *56*, 113–132.
34. Lazzarotto, L.; Dubar, L.; Ravassard, P.; Dubois, A.; Oudin, J. Identification of Coulomb's friction coefficient in real contact conditions applied to a wire drawing process. *Wear* **1997**, *211*, 54–63. [CrossRef]
35. Nikolai, L.S.; Andrey, V.F.; Sergei, Y.T.; Tarasov, I.D.; Evgeny, V.S.; Aleksandr, S.G. Acoustic emission characterization of sliding wear under condition of direct and inverse transformations in low temperature degradation aged Y-TZP and Y-TZP-Al_2O_3. *Friction* **2018**, *6*, 323–340.
36. Ji, Z.; Zhang, L.; Xie, G.; Xu, W.; Guo, D.; Luo, J.; Prakash, B. Mechanical and tribological properties of nanocomposites incorporated with two-dimensional materials. *Friction* **2020**, *8*, 813–846. [CrossRef]